Modeling of thermal spin transport and spin-orbit effects in ferromagnetic/nonmagnetic mesoscopic devices

Abraham Slachter,* Frank Lennart Bakker, and Bart Jan van Wees
Physics of Nanodevices, Zernike Institute for Advanced Materials, University of Groningen, The Netherlands
(Received 17 July 2011; revised manuscript received 19 October 2011; published 9 November 2011)

In this article we extend the currently established diffusion theory of spin-dependent electrical conduction by including spin-dependent thermoelectricity and thermal transport. Using this theory, we propose experiments aimed at demonstrating novel effects such as the spin-Peltier effect, the reciprocal of the recently demonstrated thermally driven spin injection, as well as the magnetic heat valve. We use finite-element methods to model specific devices in literature to demonstrate our theory. Spin-orbit effects such as the spin-Hall effects are also included in this model.

DOI: 10.1103/PhysRevB.84.174408 PACS number(s): 72.15.Jf, 72.25.Ba, 85.75.−d, 85.80.−b

I. INTRODUCTION

Spintronics uses the spin degree of freedom to demonstrate new functionality in ferromagnetic/nonmagnetic hybrid devices.[1] In time, many new functional devices have been proposed[2–4] and measured[5–8] utilizing the special properties of spin transport. Recently, the coupling between thermoelectricity and spin transport has been added to this field. New applications resulting from this coupling are summarized under the branch called spin-caloritronics.[7,9–15]

A diffusive transport theory for spin-dependent electrical conduction is currently well established.[16,17] This theory has been extended to noncollinear systems,[18,19] which becomes relevant when spin-dependent tunneling through interfaces is considered or to quantify dynamic processes such as spin-transfer torque[20] or spin-pumping.[3,21]

In this article, we extend the collinear theory of diffusive transport for spin-dependent conduction to include spin-dependent thermoelectricity,[22–25] spin-orbit effects,[8,26,27] and spin-dependent thermal transport.[28] We use finite-element methods to demonstrate our theory and extract useful parameters from complex three-dimensional device geometries.[27,29–32] Various recent experiments are taken from literature to extract the parameters that govern the effects. In our modeling, we ignore ballistic transport, which may give rise to (negative) nonlocal background resistances in the devices, in particular at low temperatures.[33]

The setup of this article is as follows. In Sec. II, we begin with a description of finite-element modeling where we specify the structure of the model and the solvers used. In Sec. III we describe how to make finite-element models that describe electrical spin-transport. We illustrate this model by calculating a recent example from literature.[34] We also show how the direct and inverse spin-Hall effect can be included and use it to model an experiment by Kimura *et al.*[26]

In Sec. IV, we introduce the thermoelectric-spin model. This model can describe the individual effects related to thermoelectricity[27,29,31] or spin-dependent electrical transport. However, the introduction of spin-dependent thermoelectric coefficients also allows us to demonstrate two new physical effects: the recently demonstrated thermal spin injection[30] and its Onsager reciprocal effect: the spin-Peltier effect.[38] Thermal spin injection describes the injection of spins in a nonmagnetic material when a heat current is sent through a ferromagnetic/nonmagnetic interface. The spin-Peltier effect describes spin-dependent heat transport across this interface due to the injection of spins in the ferromagnetic material.

In Sec. V, a phenomenological theory for spin-dependent heat transport is proposed, where the concept of a spin temperature is introduced as well as the thermal analogy of the spin valve—the magnetic heat valve.[10] We apply the model on a previously measured sample[27] to determine an upper limit for the relaxation of spin-dependent heat at room temperature. Thermoelectricity not only connects spin-dependent charge transport to heat transport but also connects spin-dependent heat transport to charge transport. This provides new ways to generate spin temperatures and to detect these. The use of two ferromagnets in the proposed measurement schemes ensures that the previously mentioned ballistic nonlocal resistances[33] do not hinder the observation of the proposed effects.[35,36]

We conclude this article with a brief discussion on how the developed diffusion theory, which is used to model spin-dependent effects, can be generalized to a circuit theory that can also describe tunneling through interfaces or noncollinear magnetizations.[18,37]

II. FINITE-ELEMENT MODELING

The finite-element modeling in this article is performed using the software package Comsol Multiphysics (version 3.5). It solves partial differential equations (PDEs) for 1-, 2-, or 3-dimensional geometries defined in a CAD drawing program. In a diffusive transport theory, the PDEs are determined by the conservation of the generalized currents for the physics considered. These can be formally derived from Boltzmann transport theory.[17,39] The fluxes, put into a vector by $\vec{J} = (J_{u_1}, J_{u_2}, ...)$, are governed by a vector of continuous variables $\vec{u} = (u_1, u_2, ...)$ through the conductance matrix $\bar{c}$:

$$\vec{J} = -\bar{c}\nabla\vec{u}. \tag{1}$$

Depending on the dimensionality n (1D, 2D, or 3D) of the finite-element model, the elements of the fluxes $J_{u_1}, J_{u_2}, ...$ are vectors themselves of size n. They determine the currents in the respective directions defined by the coordinate system of the model. The elements of the conductance matrix $\bar{c}(i, j)$ are then $n \times n$ matrices. For an isotropic model, these are scalar matrices, while for anisotropic transport, the elements

can be different. The PDEs in the bulk are determined by the conservation of fluxes:

$$\vec{\nabla} \cdot \vec{J} = \vec{f}(\vec{u}), \tag{2}$$

where a source term $\vec{f}(\vec{u})$ exists, which may depend on the variables themselves. As an example, for simple electrical transport $\vec{u} = V$, $\vec{J} = J_c$, $\bar{c} = \sigma$, and $f = 0$. Here V is the voltage, J_c the charge current, and σ the electrical conductivity. Equation (1) then states Ohm's law, while Eq. (2) is the Poisson equation representing the conservation of charge. The system under consideration is solved by stating the boundary conditions. These can be set for each variable (a Dirichlet condition) or flux (a Neumann condition) individually. In our example of electrical conduction, a charge current can be sent through the material by setting the charge current to a specific value at one interface and the voltage to a specific value at another. The outer interfaces are insulating $J_c = 0$ and the currents are continuous across internal interface $J_c|_1 = J_c|_2$.

A (tetrahedral) mesh of typical 300k elements is created by the finite-element program, where specific detailed meshing is used in the areas of interest by specifying a minimal element size. The PDEs are solved using a built-in (nonlinear) solver that uses the iterative generalized minimal residual solver (FGMRES) with a geometric multigrid preconditioner, which in its turn uses a direct sparse object-oriented linear equations solver (SPOOLES).

The models we use are generally nonlinear and the device on which the model is based is measured electrically. Therefore, the resulting measurable voltage is also nonlinear:

$$V = R_1 I + R_2 I^2 + R_3 I^3 + \cdots \tag{3}$$

The contributions $R_n(V/A^n)$ to the nonlinear voltage can be separately determined from experiments. By using multiple lock-in systems that are set to measure the different responses $\omega, 2\omega, 3\omega$ resulting from a sinusoidal charge current I of frequency ω sent through the device, it is possible to determine these contributions.[30] We may extract them from the constructed model by studying how the simulated voltages depend on the applied charge current. The nonlinear contributions $R_n(V/A^n)$ are determined by calculating the model at various currents and solving Eq. (3). Here the used currents are typically of a size used in experiments where all interesting contributions $R_n(V/A^n)$ are considerable.

III. SPIN TRANSPORT

Spin-dependent electron transport in systems consisting of collinear magnetizations and clean ferromagnetic/nonmagnetic interfaces is commonly described in terms of a two-channel model. First suggested by Mott,[16] and later derived from the Boltzmann transport theory,[17] it describes electrical conductance separately for spin-up (↑) electrons, the component parallel to a magnetization, and spin-down electrons (↓), the antiparallel component. Each channel has its own conductivity $\sigma_{\uparrow,\downarrow}$, voltage $V_{\uparrow,\downarrow}$, and charge current $J_{\uparrow,\downarrow}$. Usually a simplified resistor model is employed to describe spin-dependent transport. While it is sufficient for many approximations, it can become inaccurate for complex three-dimensional structures.[40]

Spin-dependent transport can be modeled by a set of PDEs by using the spin-dependent voltages as variables $\vec{u} = (V_\uparrow, V_\downarrow)$. The spin-dependent currents $\vec{J} = (J_\uparrow, J_\downarrow)$ are then defined through Eq. (1) by the spin-dependent conductance matrix:

$$\bar{c} = \begin{pmatrix} \sigma_\uparrow & 0 \\ 0 & \sigma_\downarrow \end{pmatrix}. \tag{4}$$

The conservation of charge current is given by $\vec{\nabla} \cdot (\vec{J}_\uparrow + \vec{J}_\downarrow) = 0$. The Valet-Fert equation $\nabla^2(V_\uparrow - V_\downarrow) = \frac{V_\uparrow - V_\downarrow}{\lambda^2}$ is derived from the conservation of spin currents. Defining a spin polarization for electrical conductance $\mathrm{P}_I = (\sigma_\uparrow - \sigma_\downarrow)/(\sigma_\uparrow + \sigma_\downarrow)$, we calculate the source term:

$$\vec{f} = \frac{(1 - P_I^2)\sigma}{4\lambda^2}(V_\uparrow - V_\downarrow) \cdot \begin{pmatrix} -1 \\ 1 \end{pmatrix}. \tag{5}$$

The inputs for this model are the specific geometry, the conductivity $\sigma = \sigma_\uparrow + \sigma_\downarrow$, spin relaxation length λ, and spin polarization P_I. These parameters can be determined from various experiments. For example, the relaxation length of nonmagnetic materials can be determined by varying the distance between two ferromagnets in a spin valve,[41] measuring spin precession[42] or embedding other materials in a spin valve.[43] From the measured magnitude of the spin valve, the spin-product $P_I \lambda_F$ of the ferromagnet is generally determined. Additional experiments can provide insight about the magnitude of the individual contributions P_I, λ_F. Angle-resolved photoemission provides information about the relaxation length λ_F of ferromagnets[44] (albeit high in the energy band), while the conductance polarization of ferromagnets P_I can be investigated by measuring the Doppler shift of spin-waves.[45]

Although the model fits the observed spin-valve signals of devices with clean interfaces very well,[34] in lateral systems the model often overestimates the observable spin-valve signals.[26,41,42] This is caused by the need to perform ion-milling prior to deposition, in order to obtain Ohmic interfaces. This possibly causes an increased surface area that decreases spin-valve signals.[40] Also, we cannot exclude that additional scattering centers are introduced near the interface due to the ion-milling process or that the interfacial scattering properties may be altered for a disordered interface.[46] For the permalloy ($Ni_{80}Fe_{20}$) ferromagnet commonly used in a lateral spin valve, the polarization is reduced from $P_I = 70\%$, determined from measured Doppler shifts or pillar experiments, to 30–50%.[41,47]

An example of the application of this model can be found in Bakker.[29] Another example of where this model can be applied is shown by Yang[34] *et al*. Here, the nonlocal spin valve geometry[41,48] is used to inject a spin current $J_\uparrow - J_\downarrow$ free of charge current (a so-called pure spin current) into a thin ferromagnet. The magnetization of this magnet is switched by the resulting spin-transfer torque.[2,20] A threshold exists for this process given in terms of the charge current that should be sent through the device.

A model of this device geometry with resulting spin voltage is shown in Fig. 1. Using the measured conductances, relaxation length of copper $\lambda_{\mathrm{Cu}} = 1\ \mu$m, and spin valve signals, we determine an effective spin polarization of $\mathrm{P}_I \approx 0.6$ from the measured spin valve signals 9–21 mΩ from a batch of

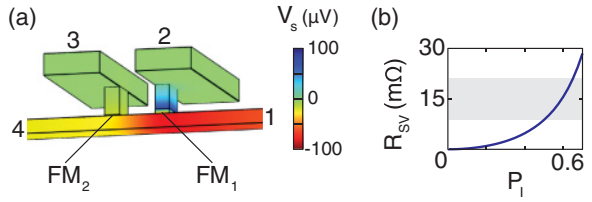

FIG. 1. (Color online) Results of the modeling of the nonlocal spin valve structure used by Yang[34] *et al.* (a) A spin current is injected into the Cu bar, which connects two ferromagnets FM_1, FM_2 by sending a charge current $I_{1-2} = 1$ mA. The injected spins diffuse toward FM_2 where they are absorbed. The color shows a calculation of spin voltage $V_s = V_\uparrow - V_\downarrow$ at $I_{1-2} = 1$ mA for the structure with a 4-nm-thin ferromagnet FM_2. (b) Calculated spin valve signal V_{3-4}/I_{1-2} (mΩ) versus the spin polarization for electrical conductance for a 20-nm-thick FM_2. The gray area shows the measured spread.

samples with thick ferromagnets. By performing an integration of the spin current flowing through the FM_2/NM interface, we find that the amount of pure spin current injected into the second ferromagnet I_s is 13.5% of the total charge current I sent through the device. For metallic F/N interfaces, the noncollinear spin injection efficiency is often comparable to the collinear spin injection efficiency.[18,46] This allows us to use this efficiency to calculate spin-transfer torque. Using an effective formula for spin-transfer torque switching,[49] we find that the ferromagnet should switch at $I_s = 930$ μA using common parameters.[6] In the experiment, the required charge current $I = 5$ mA results in a spin current of $I_s = 675$ μA. Considering the empirical spread found for the spin valve signals, this is very reasonable.

Because the electrical current density spread throughout the device is modeled, the Biot-Savart law also allows us to calculate the magnetic fields present in the device. This magnetic field is determined by performing a volume integral over the entire device. We find that the magnetic field at the center of the switchable ferromagnet is $|\vec{B}| = 1.2$ mT at the maximum applied charge current of 5 mA, while the switching field of the magnet is 8 mT. This directly rules out that the magnetization switches by the induced magnetic fields, but it can be responsible for observed asymmetries in the spin-transfer torque switching process.

A. Spin-Hall effect

Spin-orbit effects in ferromagnets are often sizable due to their intricate band alignment. As a result, measurements on spin-orbit effects in ferromagnets were already reported more then a century ago.[50] First D'Yakanov and Perel[51] and later Hirsch[4] suggested that the same process that governed these effects in ferromagnets, whether it be due to band alignment (intrinsic) or spin-dependent scattering (extrinsic),[52] can also be responsible for a new effect in paramagnetic materials: the spin-Hall effect.[8,53]

The direct spin-Hall effect describes that when a charge current J_c is sent through a material with strong spin-orbit interaction, a spin current J_s flows away from the center of the conductor with its spin direction $\vec{m}$, a unity vector, perpendicular to the charge and spin current. In the inverse version, a spin current flowing through the material creates a voltage perpendicular to the spin and spin current direction. Based on a Boltzmann transport theory derived by Zhang,[39] the effects are governed by the following two equations:

$$\vec{\nabla} V^{SH} = -\frac{\theta_{SH}}{\sigma}\vec{m} \times \vec{J}_s, \tag{6}$$

$$\vec{\nabla} V_s^{ISH} = \frac{\theta_{SH}}{\sigma}\vec{m} \times \vec{J}_c. \tag{7}$$

Here, $\vec{\nabla} V^{SH}$ and $\vec{\nabla} V_s^{ISH}$ are the bulk charge and spin voltages resulting from the direct and inverse spin-Hall effect, and θ_{SH} is the spin-Hall angle, typically $\ll 1$. Both effects can be included into the two-channel model. To do this, we rewrite both equations into spin-up and spin-down currents and obtain the new spin-dependent conductance matrix:

$$\bar{c} = \begin{pmatrix} \sigma_\uparrow & \sigma_\downarrow^{SH} \\ \sigma_\uparrow^{SH} & \sigma_\downarrow \end{pmatrix}, \tag{8}$$

where nondiagonal elements $\sigma_{\uparrow,\downarrow}^{SH}$ are included. These become skew-symmetric matrices determined by the spin-direction $\vec{m}$ considered in the device:

$$\sigma_{\uparrow,\downarrow}^{SH}(i,j) = \mp\theta_{SH}\sigma_{\uparrow,\downarrow}\sum_k \varepsilon_{ijk} m_k. \tag{9}$$

Here, (i,j,k) are the indices of the predefined xyz axes, and ε_{ijk} is the Cevi-Levita symbol.

To demonstrate the theory, we model a device measured by Kimura*et al.*,[26] where both the direct and inverse spin-Hall effect were measured in a single nanoscale device at room temperature for the first time. The results from this model are shown in Fig. 2. The device consists of a single permalloy ferromagnet, which is connected to a 4-nm-thin platinum strip by a copper cross. A pure spin current can be injected into the platinum strip by sending a charge current I_{1-2} from the ferromagnet to one of the arms of the copper cross. When the magnetization of the ferromagnet is aligned in the $\pm y$ direction, the spin current flowing into the platinum in the $-z$ direction creates a voltage due to the inverse spin-Hall effect in the x direction. This voltage can be measured between the two contacts present on the platinum strip. In the same device, sending a charge current through the platinum strip creates a spin current flowing in the z direction where the spins are aligned in the $\pm y$ direction, which is now due to the direct spin-Hall effect. When this spin current arrives at the permalloy strip, it is converted into a voltage which can be electrically measured.

Both the direct and inverse spin-Hall signal in this device are around 60 $\mu\Omega$ at room temperature at a distance of 400 nm from platinum strip to ferromagnet. Using the common parameters $P_{Py} = 0.3$, $\lambda_{Py} = 5$ nm, $\lambda_{Pt} = 2$ nm, and $\lambda_{Cu} = 350$ nm,[40,41,47] and the measured conductivities, we find that a spin-Hall angle for platinum of $\theta_{SH}^{Pt} = 5{\cdot}10^{-2}$ accurately models both signals. This angle is around 8 times smaller than previously calculated. The difference between the spin-Hall angle found by the three-dimensional model and the analysis of Kimura *et al.*[26] is partially caused by the difference in used parameters.[54] However, it is mostly due to the inaccuracy of the bulk resistor model and spin-Hall formula[39] for three-dimensional structures used in the analysis of Kimura. The

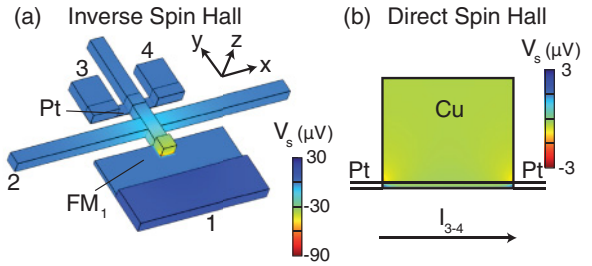

FIG. 2. (Color online) Calculated spin voltages V_s (μV) for the device of Kimura *et al.*[26] (a) In the direct spin-Hall configurations a charge current $I_{1-2} = 1$ mA is sent from ferromagnet to copper arm and the resulting spin-Hall voltage V_{3-4} is measured on the Pt strip. (b) *XZ* cross section in the middle of the platinum strip in the inverse spin-Hall configuration. The charge current $I_{3-4} = 50\ \mu$A is short-circuited by the copper strip, which is why most spin accumulation enters through the corners. When the spin voltage enters the copper strip, it is only a small fraction of the $\pm 8\ \mu$V spin voltage present in the bulk platinum. The voltage V_{1-2} is now measured by converting the spin voltage V_s to a charge voltage at the FM/NM interface.

bulk resistor model is essentially an approximation of the diffusion model we use to model the device.[32] It is known that this approximation can be too coarse in specific three-dimensional cases.[40] To illustrate the three-dimensional nature of this device, we note that only 1% of the charge current goes fully through the platinum strip when the current is sent from contact 3 to 4, because the copper on top of the strip essentially short-circuits the strip. This causes a highly nonuniform spin injection (and for the inverse effect, detection) at the platinum strip, which is illustrated by the cross section in Fig. 2(b). This example clearly demonstrates the need for a three-dimensional model to accurately fit the relevant parameters.

IV. THERMOELECTRICITY AND SPIN

Thermoelectricity[55] extends charge transport theory and includes effects governed by the Seebeck, Peltier, and thermal conductivity coefficients. We have recently shown that thermoelectric effects can be accurately modeled in nanoscale devices.[27,29–31] In this modeling, we have also included transport effects due to spin-orbit interaction by adding anisotropic elements to the conductivity and Seebeck coefficient matrices. We note that by symmetry, we expect equivalent anisotropic contributions to the Seebeck, Peltier, and thermal conductivity. However, specific measurements demonstrating the related transport effects have not been reported to the author's knowledge.

The spin-transport model extends charge transport theory to include the spin-dependency of the conductivity and introduces the concept of spin-dependent voltages $V_{\uparrow,\downarrow}$. The model which extends charge transport theory to include both thermoelectricity and spin-transport is named the thermoelectric-spin model. It has been used for almost 50 years to describe thermoelectricity in ferromagnets[56] and more recently, to describe thermoelectricity of multilayered spin valves[24,37,57] and spin transport in ferromagnets.[7,11,12]

The relevant physics and measurable voltages in devices can be calculated using finite-element modeling. The spin-dependent voltages and temperature are the variables $\vec{u} = (V_\uparrow, V_\downarrow, T)$ and the fluxes are determined by the spin-dependent charge currents and heat current $\vec{J} = (J_\uparrow, J_\downarrow, Q)$. The conductance matrix now allows us to include spin-dependent Seebeck $S_{\uparrow,\downarrow}$ and Peltier coefficients $\Pi_{\uparrow,\downarrow}$ to describe not only the coupling between charge and heat transport but also the coupling between spin and heat transport. The conductance matrix is given by

$$\bar{c} = \begin{pmatrix} \sigma_\uparrow & 0 & \sigma_\uparrow S_\uparrow \\ 0 & \sigma_\downarrow & \sigma_\downarrow S_\downarrow \\ \sigma_\uparrow \Pi_\uparrow & \sigma_\downarrow \Pi_\downarrow & k \end{pmatrix}. \tag{10}$$

The conservation of charge currents remains unchanged. However, the Valet-Fert equation is altered because in the derivation thermoelectricity is disregarded. It is originally derived using particle conservation:[58]

$$\frac{1}{e}\nabla \cdot J_{\uparrow,\downarrow} = \mp \frac{n_\uparrow}{\tau_{\uparrow\downarrow}} \pm \frac{n_\downarrow}{\tau_{\downarrow\uparrow}}. \tag{11}$$

Here $\tau_{\uparrow\downarrow}$ represents the time for a spin-up electron to flip its spin to spin down while $\tau_{\downarrow\uparrow}$ represents the time from a spin-down electron to flip its spin to spin up. The excess electron densities are given by the Einstein relation for metals $n_{\uparrow\downarrow} = N_{\uparrow\downarrow} e V_{\uparrow\downarrow}$, with $N_{\uparrow\downarrow}$ the spin-dependent densities of states at the Fermi energy. In the thermoelectric-spin model, the spin-dependent charge currents $J_{\uparrow,\downarrow} = -\sigma_{\uparrow,\downarrow}(\nabla V + S_{\uparrow,\downarrow}\nabla T)$ additionally includes a temperature gradient as well as the spin-dependent Seebeck coefficients.

The Seebeck coefficient describes how the conductivity depends on energy and is described by the Mott formula.[59] By virtue of the Einstein relation for metals, the Seebeck coefficient is determined by the energy derivative of the density of states $(\frac{dN}{dE})_{E_F}$ and the relaxation time $(\frac{d\tau}{dE})_{E_F}$ at the Fermi energy. To develop an altered Valet-Fert equation, the energy dependence of the densities of states $N_{\uparrow,\downarrow}$ and relaxation times $\tau_{\uparrow\downarrow,\downarrow\uparrow}$ needs to be taken into account at the right side of Eq. (11). While theoretically these contributions can be taken into account, in practice not much is known about these specific energy dependencies. For simplicity, we ignore such terms in the modeling and note that they can be responsible for small bulk source terms.[7,30] Conservation of charge, spin, and heat currents are now taken directly from the individual thermoelectric and spin-transport models and produce the following source term:

$$\vec{f} = \begin{pmatrix} \frac{\left(1-P_I^2\right)\sigma}{4\lambda^2}(V_\uparrow - V_\downarrow) \\ -\frac{\left(1-P_I^2\right)\sigma}{4\lambda^2}(V_\uparrow - V_\downarrow) \\ J_\uparrow^2/\sigma_\uparrow + J_\downarrow^2/\sigma_\downarrow + \sigma\frac{1-P_I^2}{4\lambda^2}V_s^2 \end{pmatrix}, \tag{12}$$

where we introduced the individual Joule heating of both spin channels $J_{\uparrow,\downarrow}^2/\sigma_{\uparrow,\downarrow}$ as well as Joule heating due to spin relaxation[14] $\nabla J_s \cdot V_s/2$.

In the spin-dependent charge transport model, the ferromagnetic/nonmagnetic interface plays a crucial role in converting spin transport into charge transport and vice versa. Using this coupling between spin and charge, magnetic memory elements can be constructed. In the thermoelectric-spin model, the ferromagnetic/nonmagnetic interface plays a similar role.

In the following we will show that this interface can be used to convert heat transport into spin transport and vice versa. The conversion of a heat current into a spin voltage depends solely on the spin-dependency of the Seebeck coefficient and is therefore named the spin-dependent Seebeck effect or by its more application oriented name: thermal spin injection.[30]

Here, we also propose a measurement scheme for the Onsager reciprocal effect. We show that when a spin current is injected into a ferromagnet a net heat flow develops, even in the absence of a charge current. This effect, named the spin-Peltier effect,[38] depends solely on the spin-dependency of the Peltier coefficient.

A. Spin-dependent Seebeck effect

The spin-dependent current model dictates that when a charge current $J_c = J_\uparrow + J_\downarrow$ is sent through the bulk of a ferromagnet, a spin current $J_s = J_\uparrow - J_\downarrow$ accompanies it of which the size is determined by the conductivity polarization $J_s = P_I J_c$.

In similar fashion, the thermoelectric-spin model dictates that when a heat current Q is sent through the bulk of a ferromagnet in the absence of a charge current, a spin current $J_s = -\sigma_F(1 - P^2)S_s\nabla T/2$ flows, of which the size is determined by the spin-dependent Seebeck coefficient $S_s = S_\uparrow - S_\downarrow = P_s S$. Here P_s is a fraction of the regular Seebeck coefficient S, defined in terms of the spin-dependent Seebeck coefficients as

$$S = \frac{\sigma_\uparrow S_\uparrow + \sigma_\downarrow S_\downarrow}{\sigma_\uparrow + \sigma_\downarrow}. \tag{13}$$

In a nonmagnetic material, both the conductivity polarization and the spin-dependent Seebeck coefficient are zero. When a charge current is sent through a ferromagnetic/nonmagnetic interface, the discontinuity in bulk spin current creates a spin voltage at the interface and injects a net spin current in the nonmagnetic material. The same situation occurs when a heat current in the absence of a charge current is sent through the interface.

This effect, the injection of spins in a nonmagnetic material by a heat current, is named thermal spin injection or, equivalently, the spin-dependent Seebeck effect.[30] Since both electrical and thermal spin injection arise from the discontinuity of the bulk spin currents, both effects have similar behavior. For example, the spin voltage spreads an equal distance away from the interface and both effects suffer from the conductivity mismatch problem,[60] which strongly reduces spin injection in low conductivity materials such as semiconductors. The possible solution to the conductivity mismatch problem is also identical: the introduction of tunnel barriers. Thermal spin injection then occurs by virtue of spin-dependent Seebeck tunneling coefficients.[13]

Thermal spin injection was recently demonstrated in a multiterminal lateral device.[30] In this device, a temperature gradient is applied to a F/N/F spin valve by Joule heating one of the ferromagnets by a large charge current. The thermoelectrically generated spin voltage across the first ferromagnetic/nonmagnetic interface is measured by a second ferromagnetic/nonmagnetic interface, which converts the spin voltage into a measurable voltage. A schematic picture of thermal spin injection and the used measurement scheme is shown in Fig. 3.

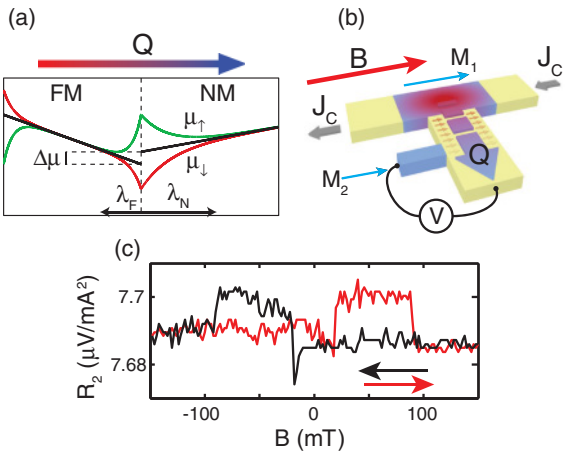

FIG. 3. (Color online) Thermal spin injection, measurement scheme, and measured result.[30] (a) A heat current sent through a F/N interface generates a spin voltage $V_s \approx \lambda_F S_s \nabla T$ at the interface which extends a distance λ_N, λ_F in the materials. (b) Thermal spin injection can be measured by Joule heating FM_1 in a lateral spin valve. This generates a heat current Q over the FM_1/NM interface which injects spins. The spin voltage is turned into a measurable voltage by the FM_2/NM interface. The size of thermal spin injection can be determined by selectively switching the magnetizations. (c) Measurement result. A signal due to thermal spin injection is present on a large background caused by the measurement of Joule heating by the FM_2/NM thermocouple. In addition, small traces of anisotropic magnetoresistive heating effects as well as anomalous-Nernst effects are present. These can be seen by the small dip at the switching field of FM_1 and the offset in background voltage between large positive and negative magnetic fields (see also Fig. 7).

Because Joule heating scales quadratically with the applied charge current I^2, thermal spin injection results in a nonlinear spin-dependent signal $R_2^s = R_2^P - R_2^{AP}$, where R_2^P and R_2^{AP} are the parallel and antiparallel contributions. The measured result is shown in Fig. 3(c). The applied temperature gradient was very limited due to the relatively large lateral size and because electromigration prohibits heating in excess of 40K in this particular case.

In addition to thermal spin injection, we observe small traces of spin-orbit effects such as the anomalous-Nernst effect in the second ferromagnet and anisotropic magnetoresistive heating of the first ferromagnet. The effects have been more thoroughly examined in another device.[27] These effects express themselves by a difference in background voltage for both parallel orientations and the observed small curve in voltage prior to the low field switch.

An application of spin currents lies in its ability to switch the (uniform) magnetization of a ferromagnet around its easy axis by means of spin-transfer torque.[20] This effect has a threshold in the spin current which needs to be injected. Since electrical and thermal spin injection have the same physical origin, the discontinuity in bulk spin current, we may directly compare the critical temperature gradient in the ferromagnet needed to switch a F/N/F spin valve by spin transfer torque to the critical charge current density. If the critical charge current density is

known, we can calculate the critical temperature gradient that is needed for the switching process:

$$\nabla T|_{\text{crit}} = \frac{2P_I}{\sigma P_s S\left(1-P_I^2\right)} J_{\text{crit}}. \tag{14}$$

Here J_{crit} is the threshold in charge current at which spin transfer torque switching takes place, σ the ferromagnetic conductivity, and $\nabla T|_{\text{crit}}$ the critical temperature gradient in the bulk ferromagnet. As an example, if we assume a critical charge current density $J_{\text{crit}} = 10^{11}$ A/m^2 for a permalloy ferromagnet, with the common (estimated) parameters $P_I = 0.6$, $P_s = 0.6$, $\sigma = 4 \cdot 10^6$ S/m, and $S = -20\,\mu V$, we find a critical temperature gradient of $\nabla T = 4 \cdot 10^9$ K/m. A typical F/N/F stack of 25 nm then switches at an applied temperature difference of 100 degrees. Recently, evidence for this process, known as thermal spin transfer torque, has been found.[61]

The ability to use finite element modeling should allow us to engineer multiterminal F/N/F pillar devices that can switch by thermal spin transfer torque. Such devices can combine the high polarization properties of pillar devices with the flexibility of lateral devices. By selectively heating the device, the effect can also be used to lower the effective threshold of spin-transfer torque switching.

B. Spin-Peltier effect

The Onsager reciprocity relation dictates that when heat transport induces spin transport free of charge currents in a ferromagnet, the opposite can also occur. A pure spin current injected in a ferromagnet should induce net heat transport. This Onsager reciprocal effect is named the spin-Peltier effect.[38]

We illustrate this effect in Fig. 4 by considering the F/N interface previously used. A pure spin current is injected from the nonmagnetic side into the ferromagnet. When the spin current enters the ferromagnet it reduces in size at the spin

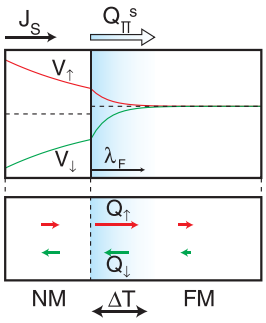

FIG. 4. (Color online) Schematic representation of the Spin-Peltier effect. A spin current $J_s = J_\uparrow - J_\downarrow$ free of charge current ($J_\uparrow + J_\downarrow = 0$) is injected from the nonmagnetic side of the F/N junction into a ferromagnet (FM). The top shows the resulting spin-dependent voltages, calculated using the two-channel model. Despite the fact that no charge current is flowing through the junction, a net heat flow $Q_\Pi^s = \frac{1}{2}(\Pi_\uparrow - \Pi_\downarrow)J_s$ develops in the ferromagnet which quickly drops off due to the spin relaxation length λ_F. Depending on the sign of the spin current and the parallel/antiparallel alignment of the magnetization, net heat is transported from the nonmagnetic material to the ferromagnet or vice versa. This creates a temperature difference ΔT between the bulk nonmagnetic material and the bulk ferromagnet.

relaxation length, for metals ranging from a few to tens of nanometers. The spin-dependent voltages that result from the spin current are sketched in the top part of Fig. 4. In the absence of charge currents, the heat current in the system due to the spin-Peltier effect Q_Π can be deduced from the thermoelectric-spin model:

$$Q_\Pi = \tfrac{1}{2}(\Pi_\uparrow - \Pi_\downarrow)J_s. \tag{15}$$

In the nonmagnetic material, $\Pi_\uparrow = \Pi_\downarrow$ and no net heat transport due to the spin-Peltier effect takes place. In the ferromagnet, the spin-Peltier coefficient, defined as $\Pi_s = \Pi_\uparrow - \Pi_\downarrow$ can be nonzero. Close to the interface, the spin current $\vec{J}_s$ is also nonzero. This induces heat transport due to the spin-Peltier effect, which drops off in the ferromagnet at the spin relaxation length. As a result, a temperature difference ΔT develops between the bulk nonmagnetic material and the ferromagnet.

The Onsager-Kelvin relation $\Pi = ST$ relates the conventional Seebeck and Peltier coefficients. This also holds for the individual spin species. From the recently found spin-dependent Seebeck coefficient S_s we can calculate the spin-Peltier coefficient $\Pi_s = S_s T$, which can be used to estimate the effect.

We calculate the exact temperature difference by considering the total heat current $Q = \frac{1}{2}\Pi_s J_s - k\nabla T$ in the ferromagnetic and nonmagnetic regions. Like spin and charge currents, the heat current is continuous across the interface. If we ignore Joule heating due to spin currents, it is also continuous in the bulk of the nonmagnetic and ferromagnetic parts and equal to $k_i \nabla T|_i$. Here the index i denotes the region. The presence of the spin-Peltier effect induces an additional temperature gradient $\nabla T|_\Pi(x) = \frac{\Pi_s}{2k_F} J_s(x)$ in the small ferromagnet region in which a sizable spin current exists. The spin current drops off exponentially from the interface: $J_s(x) = J_s^0 e^{-x/\lambda_F}$. Here J_s^0 is the spin current at the interface. If we integrate this additional temperature gradient over this region, we find the temperature difference between the bulk ferromagnet and nonmagnetic material:

$$\Delta T|_{F-N} = \frac{\Pi_s}{2k_F}\lambda_F J_s^0. \tag{16}$$

This temperature difference depends solely on the spin-Peltier coefficient Π_s, the spin relaxation length λ_F, and the thermal conductivity k_F of the ferromagnet. Its sign is determined by the sign of spin current and the spin-Peltier coefficient.

The nonlocal spin valve geometry is an ideal geometry to inject pure spin currents into a ferromagnet. The generated temperature difference over the interface can be detected by measuring the temperature of the ferromagnet in which the pure spin current is injected. This can be achieved by placing a thermocouple on the ferromagnet. This measurement geometry is illustrated in Fig. 5. The background voltage is then solely determined by the Peltier heating of the FM_1/NM interface, which injects the spin current and the subsequent measurement of the temperature by the thermocouple. The spin-Peltier signal then appears as a regular resistance R_1,

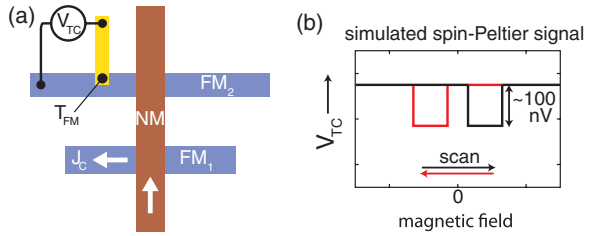

FIG. 5. (Color online) Proposed nonlocal measurement scheme for the spin-Peltier effect. (a) The nonlocal spin valve geometry allows us to inject a pure spin current into ferromagnet FM_2 by sending a charge current J_c across the FM_1/NM interface. This spin current creates a temperature difference across the FM_2/NM interface changing the local temperature T_F of the ferromagnet. The effect is detected by converting the temperature to a voltage $V_{TC} = \Delta S_{FM} T_F$ using a thermocouple. Here ΔS_{FM} is the difference between Seebeck coefficients between the ferromagnet and the nonmagnetic material (yellow). The thermocouple measures the temperature T_F of the ferromagnet and, optionally, makes use of the large Seebeck coefficient of the ferromagnet itself. (b) The simulated spin-Peltier signal. The resulting signal should have a background determined by Peltier cooling/heating at the FM_1/NM interface and subsequent consequence to the temperature T_F. A small signal of 100 nV due to the spin-Peltier effect should arise which only depends on the parallel or antiparallel alignment of both magnetizations.

which depends on the parallel or antiparallel alignment of both magnetizations.

For permalloy, all parameters are known[30] and we can estimate the temperature difference that can be created in this manner. At a realistic maximum pure spin current that can be injected into a permalloy ferromagnet in the nonlocal spin valve geometry (see the previous discussion below Fig. 1) we have $J_s^0 = 10^{11}$ A/m^2. Using this value, we find a temperature difference of $\Delta T = 20$ mK between the parallel and antiparallel orientation of the permalloy spin valve across the interface of the ferromagnet. A typical thermocouple that can be realized on a (lateral) ferromagnet[27] has an efficiency of $\Delta S = 40 \mu V/K$. This results in a maximal spin-Peltier signal of 800 nV, which is small but observable. Initial experiments show signs of the spin-Peltier effect; however, it is hard to distinguish it from small parasitic effects, for example, the pick-up of regular nonlocal spin valve signals by an uneven distribution of the spin-voltage at the detecting interface.[62]

V. BEYOND THERMOELECTRICITY AND SPIN: THE SPIN-DEPENDENT HEAT MODEL

In the thermoelectric-spin model a single electron temperature was introduced which holds for both spin species. The energy of the electrons is distributed in their respective bands according to a position-dependent Fermi-Dirac distribution $f_{\uparrow,\downarrow}(\epsilon, n_{\uparrow}, T)$ with a spin-specific local density $n_{\uparrow,\downarrow}$ and local temperature T. This model requires strong (spin-conserving) inelastic interaction between spins to obtain the required thermodynamic distribution. This requirement must hold for the individual spin species, but also strong inelastic interaction must be present between the spin species, such that the temperatures of the individual spin species are equal. It is caused by electron-electron interaction or mediated by phonons through electron-phonon interaction.

At low temperatures inelastic scattering becomes weaker and this requirement does not hold. It was shown in the past that inelastic scattering can be weak on the scale of the spin relaxation length in nonmagnetic metals[63] at sub-4K temperatures where electron transport is still diffusive, limited by elastic scattering. Although in this situation it is hard to speak of electrons that are distributed according to a Fermi-Dirac distribution in their respective bands, it is still possible to describe thermal transport according to a diffusion equation. The temperature T then represents the local average excess energy of electrons compared to the situation at zero Kelvin. In addition, the spin-dependent electron species also do not exchange energy with each other.

This requires the introduction of a spin-dependent heat model where both spin channels have their own heat current $Q_{\uparrow,\downarrow}$, thermal conductivity $k_{\uparrow,\downarrow}$, and spin-dependent temperature $T_{\uparrow,\downarrow}$. This opens up the possibility to demonstrate new thermal and, possibly, thermoelectric experiments in magnetoelectronic devices. Such a model has first been described by Heikkilä *et al.*[10] We introduce a bulk diffusion model and calculate a specific device to provide an example.

The Wiedemann-Franz law $L = \frac{k}{\sigma T}$ describes the relation between charge and thermal conductivity for metals at different temperatures. Here $L \approx 2.4 \cdot 10^{-8}\,\mathrm{W\Omega K^{-2}}$ is the Lorenz number, which varies mildly between metals.[64] The law assumes that the thermal conductivity is determined by electron transport, which is often the case in metals.[65] The relation can be used to estimate thermal conductivities from measured charge conductivities. Because the charge and thermal conductivity are often determined by electron transport, a spin polarization in the electrical conductance P_I naturally leads to a spin polarization in thermal conductance P_Q, similarly defined in terms of spin-dependent heat conductances as $P_Q = (k_{\uparrow} - k_{\downarrow})/(k_{\uparrow} + k_{\downarrow})$. The model for spin-dependent electrical and thermal transport now includes the spin-dependent voltages and temperatures $\vec{u} = (V_{\uparrow}, V_{\downarrow}, T_{\uparrow}, T_{\downarrow})$. The spin-dependent charge and heat currents $\vec{J} = (J_{\uparrow}, J_{\downarrow}, Q_{\uparrow}, Q_{\downarrow})$ are determined through the 4×4 conductance matrix

$$\bar{c} = \begin{pmatrix} \sigma_{\uparrow} & 0 & \sigma_{\uparrow} S_{\uparrow} & 0 \\ 0 & \sigma_{\downarrow} & 0 & \sigma_{\downarrow} S_{\downarrow} \\ \sigma_{\uparrow} \Pi_{\uparrow} & 0 & k_{\uparrow} & 0 \\ 0 & \sigma_{\downarrow} \Pi_{\downarrow} & 0 & k_{\downarrow} \end{pmatrix}, \qquad (17)$$

where the spin-dependent thermoelectric effects, represented by the coefficients $S_{\uparrow,\downarrow}$ and $\Pi_{\uparrow,\downarrow}$, are used in the relevant spin-dependent currents. The conservation of spin and charge currents remains the same, and therefore the components of the source term for the spin-dependent charge currents as well. It is straightforward to include the conservation of the total heat current $Q = Q_{\uparrow} + Q_{\downarrow}$ into its spin-dependent parts: the Joule heating of each channel $J_{\uparrow,\downarrow}^2/\sigma_{\uparrow,\downarrow}^2$ simply applies to the channels individually. We note here that, strictly speaking, if there is no inelastic scattering, there is no Joule heating. However, any weak inelastic scattering does raise the average energy of the electron baths, which allows Joule heating to be used in the model as a local source of heat.

Although it is beyond the scope of this article to derive the conservation of spin heat currents $Q_s = Q_\uparrow - Q_\downarrow$ from Boltzmann transport theory,[14] we may introduce a phenomenological relaxation analog to the relaxation of the amount of spins themselves, represented by the Valet-Fert equation for spin voltage.

The difference in excess energy between both spin species is represented by the spin temperature $T_s = T_\uparrow - T_\downarrow$. In our model, we assume a thermal equivalent of the Valet-Fert equation $\nabla^2 T_s = \frac{T_s}{\lambda_Q^2}$. Here λ_Q is the relaxation length for the spin temperature. This relaxation length is not only limited by spin flip processes but can also be limited due to inelastic scattering between both spin species, where energy is being exchanged between both spin species without flipping its spin. This results in the boundary condition for spin relaxation lengths $\lambda_Q \leqslant \lambda$. The spin relaxation lengths are equal whenever inelastic scattering is absent.

New source terms $\pm\frac{(1-P_Q^2)k}{4\lambda_Q^2}(T_\uparrow - T_\downarrow)$ are then added such that the conservation of spin heat is also included. This leads to the following source term in this model:

$$\vec{f} = \begin{pmatrix} \frac{(1-P_I^2)\sigma}{4\lambda^2}(V_\uparrow - V_\downarrow) \\ -\frac{(1-P_I^2)\sigma}{4\lambda^2}(V_\uparrow - V_\downarrow) \\ \frac{(1-P_Q^2)k}{4\lambda_Q^2}(T_\uparrow - T_\downarrow) + J_\uparrow^2/\sigma_\uparrow + \sigma\frac{1-P_I^2}{8\lambda^2}V_s^2 \\ -\frac{(1-P_Q^2)k}{4\lambda_Q^2}(T_\uparrow - T_\downarrow) + J_\downarrow^2/\sigma_\downarrow + \sigma\frac{1-P_I^2}{8\lambda^2}V_s^2 \end{pmatrix}. \quad (18)$$

The thermoelectric coefficients in this model typically scale with temperature and are very small at the temperatures where this model is applicable. For example, for many nonmagnetic metals the Seebeck coefficient scales linearly with temperature such that typical Seebeck coefficients are in the order of 10 nV/K at Helium temperatures.[56] This also holds for typical ferromagnets such as cobalt or permalloy. Due to the small size of these coefficients, the nonlocal background voltages at these temperatures will likely not be determined by thermoelectricity but by ballistic transport[33] or conventional Ohmic voltages. Therefore, we first disregard (spin-dependent) thermoelectricity and explore the special properties of spin-dependent heat itself by proposing the thermal equivalent of the spin valve.

A. Magnetic heat valve

If we disregard thermoelectricity as well as charge currents in magnetoelectronic devices, such that Joule heating is absent, spin-dependent charge and heat transport are each represented by an independent set of equations. The mathematical model introduced to describe spin-dependent heat transport is then identical to that which describes spin-dependent charge transport. The difference between the models is the size of the coefficients. The equivalence of the coefficients used in both models is depicted in Fig. 6(a).

Consequently, concepts which are relevant in the spin-dependent charge transport model will have their equivalent in the spin-dependent heat transport model. A similar resistor model also applies.[17] For example, consider a heat current Q sent through a F/N interface. This creates a difference in temperature between both spin species T_s which relaxes in the materials with the spin heat relaxation length λ_Q. This is depicted in Fig. 6(b). The size of the spin temperature at the interface can be directly deduced from the equivalently calculated spin voltage V_s in the charge transport model:[66]

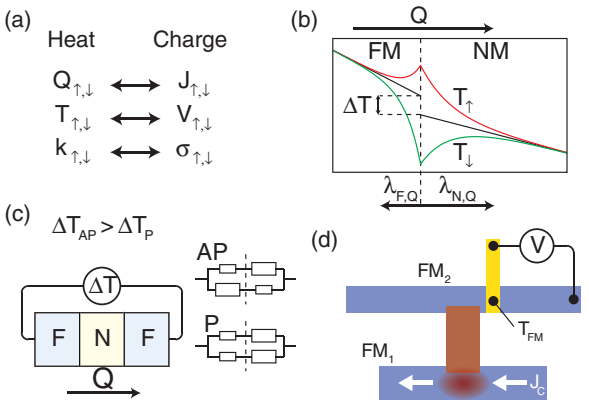

FIG. 6. (Color online) The spin-dependent heat model. (a) Equivalency between the coefficients of the spin-dependent heat and charge models when thermoelectricity and Joule heating is disregarded. (b) A heat current Q sent through the F/N interface creates a spin-temperature T_s and spin-related temperature difference ΔT. (c) The F/N/F magnetic heat valve. A heat current sent through a F/N/F spin valve structure creates a temperature difference across it dependent on the parallel or antiparallel alignment of both magnetizations. (d) A possible experimental realization of the F/N/F heat valve. By heat sinking one ferromagnet and Joule heating another, heat can be transported through the heat valve. The temperature of the second ferromagnet depends on the specific thermal resistance of the heat valve, determined through the parallel or antiparallel alignment of the magnetizations, and can be measured using a thermocouple.

$$\frac{T_s}{Q} = \frac{2P_Q R_{F,Q} R_{N,Q}}{R_{F,Q} + (1-P_Q^2)R_{N,Q}}, \quad (19)$$

where $R_{N,Q} = \frac{\lambda_{N,Q}}{k_N}$ and $R_{F,Q} = \frac{\lambda_{F,Q}}{k_F}$ are the equivalent thermal resistances determined by the spin heat relaxation lengths and the thermal conductivities of the materials. A spin related "thermal resistance" $\Delta T = \frac{1}{2}P_Q T_s$ also develops across the interface.

There also exists a thermal equivalent of the electrical F/N/F spin valve. When a heat current Q is sent through a F/N/F spin valve, a temperature difference ΔT develops across it, which depends on the parallel or antiparallel alignment of the magnetizations. We refer to this concept as the magnetic heat valve. It is depicted in Fig. 6(c). In the electrical spin valve, a simple calculation[41] gives the difference between parallel and antiparallel resistance per unit area $R_P - R_{AP} = 2P_I^2 R_F R_N/[R_F + R_N(1-P_I^2)]$ whenever the distance L between both ferromagnets is $L \ll \lambda_N$. Whenever $L \ll \lambda_{N,Q}$ we obtain the temperature difference between the parallel and antiparallel alignment in the magnetic heat valve:

$$\frac{\Delta T_P - \Delta T_{AP}}{Q} = \frac{2P_Q^2 R_{F,Q} R_{N,Q}}{R_{F,Q} + R_{N,Q}(1-P_Q^2)} \quad (20)$$

As an example, let us consider a Py/Cu/Py heat valve in a 25-nm-thick pillar stack where the nonmagnetic metal is thin enough to satisfy the condition $L \ll \lambda_{N,Q}$. Whenever

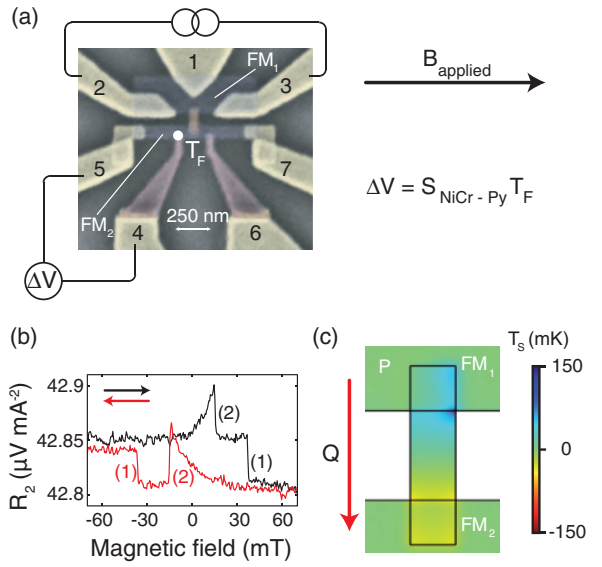

FIG. 7. (Color online) Modeling of a fabricated device[27] that potentially could show the magnetic heat valve effect. (a) SEM figure and measurement geometry. Two permalloy ferromagnets (blue) are connected by a copper rectangle (brown). The temperature T_F of the second ferromagnet is measured by a NiCr (contact 4,6)/Py thermocouple. (b) Measurement at a typical current of 1 mA. No regular spin valve signal is present, which would be the result of the magnetic heat valve effect. The anomalous-Nernst (1) and anisotropic magnetoresistive heating (2) effects are present. (c) Calculated spin temperature at $I_{1-2} = 1$ mA zoomed at the copper rectangle calculated using the parameters $\lambda_{Py,Q} = 5$ nm, $\lambda_{Cu,Q} = 350$ nm, and $P_Q = 0.25$.

the spin valve is held at a total temperature where inelastic scattering is small but not negligible, say $\lambda_Q \approx \lambda/2$ and assume the estimated values $P_Q = 0.6, \lambda_F = 5$ nm, $\lambda_N = 1\mu$m, $k_{Cu} = 300$ W/m/K, $k_{Py} = 30$ W/m/K an applied heat current of $Q = k_{Py} \cdot 10\text{K}/25\text{nm} = 1.2 \cdot 10^{10}$ W/m^2 produces a significant temperature difference of $\approx$2K across the spin valve depending on the parallel or antiparallel alignment.

In a spin valve, it is possible to use Joule or laser heating to produce heat currents through a device.[57] However, measuring a temperature difference across a device is nontrivial. Nevertheless, by measuring the absolute temperature at the second ferromagnet with the aid of a thermocouple, the process can be measured, because the process does influence the net heat flow through the device. This experimental measurement technique is sketched in Fig. 6(d). It is fairly nontrivial to use analytical solutions, as heat transport through a substrate and Joule heating itself are hard to calculate in a three-dimensional geometry. However, by fitting the obtained measured voltages to those resulting from a finite-element model with varying geometry, it should be possible to extract useful coefficients, such as spin heat relaxation lengths at different temperatures.

This experimental measurement technique has been used previously at room temperature.[27] Here, a Py/Cu/Py spin valve and a Py/NiCr thermocouple were used. A SEM picture of the device is shown with a typical measurement in Fig. 7. The system was modeled with a regular thermoelectric model, which showed that a maximum heat current of $Q \approx 10^9$ W/m^2 can be achieved at which the temperature difference across the spin valve is $\approx$2K with a used charge current of $I_c = 2$ mA.

Although at room temperature, regular spin-orbit effects such as the anomalous-Nernst (1) and anisotropic magnetoresistance (2) are dominant, we can use this sample to demonstrate a calculation of the spin-dependent heat model. Using the additional parameters shown in Fig. 7, and assuming no inelastic scattering ($\lambda_Q = \lambda$) and $P_Q = P_1$, we calculate a temperature difference $\Delta T_P - \Delta T_{AP} = 8$ mK due to the heat valve effect which leads to a response $R_2^s = 19.6$ nV/mA^2 when the thermocouple is measured. The temperature difference is 10 times lower than the value calculated from Eq. (20) with $\nabla T|_F \approx 3 \cdot 10^7$ K/m and is due to spin relaxation in the nonmagnetic material. With a noise level of $\approx$5 nV/mA^2, the heat valve effect should be observable if inelastic scattering between both spin species is absent. The absence of a spin heat signal above the noise level shows that inelastic scattering is strong enough such that we find the requirement $\lambda_Q < \frac{1}{2}\lambda$ valid at room temperature. When $\lambda_Q = \frac{1}{2}\lambda$, the calculated signal is approximately identical to the noise level.

B. Thermoelectricity and spin-dependent heat

The spin-dependent heat model becomes relevant when inelastic interaction between the spin species is weak, which occurs at low temperatures. Thermoelectric effects are small at these temperatures and ballistic effects sizable,[33] which is why thus far we did not consider the connection between the spin-dependent thermoelectric effects and the effects due to spin-dependent heat.

However, prospects in fabrication that connects the flexibility of a multiterminal lateral device design with the high signals observed in pillar structures and the low noise experiments associated with a low operating temperature should increase the observability of the effects so far considered. We may then also consider the higher-order effects related to this connection.

Whenever a charge current J_c is sent through a ferromagnet, a spin heat current $Q_s = \Pi_s J_c$ also flows, determined by the spin-Peltier coefficient Π_s. Here we assumed $V_\uparrow = V_\downarrow$. Similar to the case of electrical- and thermal-spin injection, when this charge current is sent through a F/N interface, this creates a spin temperature T_s^0 at the interface which relaxes in the respective materials at the respective spin heat relaxation lengths λ_Q. We propose to name this effect the thermal spin-Peltier effect. The size of the effect is given by Eq. (19) with the source of the spin heat current in the bulk $Q_s = P_Q Q$ substituted by that due to this effect $Q_s = \Pi_s J_c$. We note that this ignores the generation of a spin voltage at the interface which by ordinary thermoelectric effects is converted to a spin temperature.

Although at low temperatures Π_s can be very small, the maximum charge current, typically limited by electromigration ($J_c^{\max} = 10^{12}$ A/m^2), is often larger than the maximum heat current. This may render this effect more efficient to generate a spin temperature than the previously described effect in the magnetic heat valve.[67]

The Onsager reciprocal effect can also occur in this model. Whenever a spin heat current Q_s is injected into a ferromagnet at a F/N interface, this creates a voltage difference $\Delta V|_{F-N}$ between the bulk nonmagnetic material and ferromagnet. We

propose to name this the thermal spin-dependent Seebeck effect. The calculation of this voltage goes similar to the calculation of the temperature difference ΔT in the spin-Peltier effect. Checking the symmetry between the spin-dependent charge and heat models we can directly substitute the various coefficients in Eq. (16) to obtain the induced voltage difference over the interface:

$$\Delta V|_{F-N} = \frac{S_s}{2k_F}\lambda_{F,Q} Q_s^0. \tag{21}$$

It is possible to measure this voltage difference directly over an interface in a multiterminal nonlocal device. However, it requires a source of pure spin heat current Q_s in which preferably a charge-related spin current J_s is absent. This is a situation difficult to achieve. However, if both sources of Q_s and J_s scale differently with applied charge current it is perhaps possible to distinguish between the generation of a voltage over a F/N interface due to charge-related spin currents and those due to spin heat currents in a suitably designed experiment.

VI. DISCUSSION

Throughout this article we have considered transparent (Ohmic) interfaces and collinear magnetic systems. In this case, the spin-dependent charge and heat currents are continuous across the interfaces and are scalar quantities. Past experiments show that whenever oxide layers are formed at interfaces the spin-dependent effects can be greatly enhanced.[68] Furthermore, a noncollinear system is required to describe important applications of spin-dependent transport such as the spin-torque-oscillator[5,69–72] or spin-transfer-torque magnetic memory.[20,34,73] In these cases the diffusion theory developed here is not sufficient to describe the relevant processes. Instead, it should be described by a more general theory that includes spin-dependent tunneling and a 3-dimensional spin vector, for example, the magnetoelectronic circuit theory.[18,19] Heikkilä, Hatami, and coworkers have previously developed such a theory[10,37,38] in order to describe thermal spin-transfer torque and spin-dependent thermal transport.

This theory essentially extends the diffusion theory used in this article. The diffusion theory uses flux and variable continuity to describe electron transport across ferromagnetic/nonmagnetic interfaces. In the noncollinear theory, this transport is described by a 4×4 conductance matrix G, which relates the total flux $\bar{J} = (J_c, \vec{J}_s, Q, \vec{Q}_s)$ at the interface to the variables at both sides $\bar{u}^i = (V_c^i, \vec{V}_s^i, T^i, \vec{T}_s^i)$ $(i = \mathrm{F}, \mathrm{N})$ by $\bar{J} = \bar{G}(\bar{u}^F - \bar{u}^N)$.

Initial calculations on the conductance matrix for F/N interfaces have been carried out by Hatami and coworkers,[37] who in this framework calculated thermal spin-transfer-torque for various ferromagnet/nonmagnetic interfaces.

In the extended magnetoelectronic circuit theory they have introduced, the spin-dependent physics such as electrical or thermal spin injection is often determined by the elements of the conductance matrix instead of the previously defined bulk spin-polarized parameters P_I, P_S, P_Π, P_Q of the ferromagnet. This difference in modeling is a matter of choice; the physics they describe is the same.

For metallic transparent ferromagnetic/nonmagnetic interfaces, the noncollinear spin injection into a ferromagnet is often comparable to collinear spin injection,[46] also for thermal spin injection.[37,38] This allows us to use the results from the obtained spin injection efficiency in the collinear diffusive case to calculate effects that are due to noncollinear spin injection, such as spin-transfer torque. We note that the difference between collinear and noncollinear spin transport may be determined by the angular dependence of the (nonlocal) spin resistance.[18] Dependent on the application, either the more simple diffusive theory developed here can be used or one needs to refer to the full circuit theory.

VII. SUMMARY

We have developed a diffusive theory for spin-dependent charge and heat conduction that includes spin-orbit effects. Finite-element methods were used to model several experiments from literature where several parameters of this model were quantified. Electrical spin injection, the spin-Hall angle of platinum, and thermal spin injection were calculated. Also, new experiments were proposed that should demonstrate the spin-Peltier effect and a lower limit was given in an experiment that failed to demonstrate the magnetic heat valve.

ACKNOWLEDGMENTS

We acknowledge J. G. Holstein, B. Wolfs, and S. Bakker for technical assistance and F. K. Dejene for critically reading the manuscript. This work was financed by European EC Contract Nos. IST-033749 "DynaMax" and ICT-251759 "MACALO" and the "Stichting voor Fundamenteel Onderzoek der Materie" (FOM).

*A.Slachter@gmail.com

[1] I. Zutic, J. Fabian, and S. Das Sarma, Rev. Mod. Phys. **76**, 323 (2004).
[2] J. Slonczewski, J. Magn. Magn. Mater. **159**, L1 (1996).
[3] A. Brataas, Y. Tserkovnyak, G. E. W. Bauer, and B. I. Halperin, Phys. Rev. B **66**, 060404 (2002).
[4] J. E. Hirsch, Phys. Rev. Lett. **83**, 1834 (1999).
[5] S. Kiselev, J. Sankey, I. Krivotorov, N. Emley, R. Schoelkopf, R. Buhrman, and D. Ralph, Nature (London) **425**, 380 (2003).
[6] M. V. Costache, M. Sladkov, S. M. Watts, C. H. van der Wal, and B. J. van Wees, Phys. Rev. Lett. **97**, 216603 (2006).
[7] K. Uchida, S. Takahashi, K. Harii, J. Ieda, W. Koshibae, K. Ando, S. Maekawa, and E. Saitoh, Nature (London) **455**, 778 (2008).
[8] S. Valenzuela and M. Tinkham, Science **442**, 176 (2006).
[9] G. E. W. Bauer, A. H. MacDonald, and S. Maekawa, Solid State Commun. **150**, 459 (2010).
[10] T. T. Heikkilä, M. Hatami, and G. E. W. Bauer, Phys. Rev. B **81**, 100408 (2010).

[11] C. M. Jaworski, J. Yang, S. Mack, D. D. Awschalom, J. P. Heremans, and R. C. Myers, Nature Mater. **9**, 898 (2010).
[12] K. Uchida, J. Xiao, H. Adachi, J. Ohe, S. Takahashi, J. Ieda, T. Ota, Y. Kajiwara, H. Umezawa, H. Kawai, G. E. W. Bauer, S. Maekawa, and E. Saitoh, Nature Mater. **9**, 894 (2010).
[13] J.-C. Breton, S. Sharma, H. Saito, S. Yuasa, and R. Jansen, Nature (London) **475**, 82 (2011).
[14] A. A. Tulapurkar and Y. Suzuki, Phys. Rev. B **83**, 012401 (2011).
[15] F. Giazotto, T. T. Heikkilä, A. Luukanen, A. M. Savin, and J. P. Pekola, Rev. Mod. Phys. **78**, 217 (2006).
[16] N. Mott and H. Wills, Proc. R. Soc. **153**, 699 (1936).
[17] T. Valet and A. Fert, Phys. Rev. B **48**, 7099 (1993).
[18] A. Brataas, G. E. W. Bauer, and P. J. Kelly, Phys. Rep. **427**, 157 (2006).
[19] Y. Tserkovnyak, A. Brataas, G. E. W. Bauer, and B. I. Halperin, Rev. Mod. Phys. **77**, 1375 (2005).
[20] C. Chappert, A. Fert, and F. Nguyen van Dau, Nat. Mater. **6**, 813 (2007).
[21] Y. Tserkovnyak, A. Brataas, and G. E. W. Bauer, Phys. Rev. Lett. **88**, 117601 (2002).
[22] M. Johnson and R. H. Silsbee, Phys. Rev. B **35**, 4959 (1987).
[23] J.-E. Wegrowe, Phys. Rev. B **62**, 1067 (2000).
[24] L. Gravier, S. Serrano-Guisan, F. Reuse, and J.-Ph. Ansermet, Phys. Rev. B **73**, 052410 (2006).
[25] J. Dubois and J-P. Ansermet, Phys. Rev. B **78**, 184430 (2008).
[26] T. Kimura, Y. Otani, T. Sato, S. Takahashi, and S. Maekawa, Phys. Rev. Lett. **98**, 156601 (2007).
[27] A. Slachter, F. L. Bakker, and B. J. van Wees, Phys. Rev. B **84**, 020412(R) (2011).
[28] F. Giazotto, F. Taddei, P. D'Amico, R. Fazio, and F. Beltram, Phys. Rev. B **76**, 184518 (2007).
[29] F. L. Bakker, A. Slachter, J.-P. Adam, and B. J. van Wees, Phys. Rev. Lett. **105**, 136601 (2010).
[30] A. Slachter, F. L. Bakker, J.-P. Adam, and B. J. van Wees, Nature Phys. **6**, 879 (2010).
[31] F. L. Bakker, J. Flipse, A. Slachter, D. Wagenaar, and B. J. van Wees, e-print arXiv:1108.1286v1.
[32] J. Hamrle, T. Kimura, T. Yang, and Y. Otani, Phys Rev. B **71**, 094434 (2005).
[33] G. Mihajlović, J. E. Pearson, M. A. Garcia, S. D. Bader, and A. Hoffmann, Phys. Rev. Lett. **103**, 166601 (2009).
[34] T. Yang, T. Kimura, and Y. Otani, Nat. Phys. **4**, 851 (2008).
[35] F. G. Monzon, H. X. Tang, and M. L. Roukes, Phys. Rev. Lett. **84**, 5022 (2000).
[36] B. J. van Wees, Phys. Rev. Lett. **84**, 5023 (2000).
[37] M. Hatami, G. E. W. Bauer, Q. Zhang, and P. J. Kelly, Phys. Rev. Lett. **99**, 066603 (2007).
[38] M. Hatami, G. E. W. Bauer, Q. Zhang, and P. J. Kelly, Phys. Rev. B **79**, 174426 (2009).
[39] S. Zhang, Phys. Rev. Lett. **85**, 393 (2000).
[40] T. Kimura, Y. Otani, and J. Hamrle, Phys. Rev. B **73**, 132405 (2006).
[41] F. J. Jedema, A. T. Filip, and B. J. van Wees, Nature (London) **410**, 345 (2001).
[42] F. J. Jedema, H. B. Heersche, A. T. Filip, J. J. A. Baselmans, and B. J. van Wees, Nature (London) **416**, 713 (2002).
[43] T. Kimura, J. Hamrle, and Y. Otani, Phys. Rev. B **72**, 014461 (2005).
[44] D. Y. Petrovykh, K. N. Altmann, H. Höchst, M. Laubscher, S. Maat, G. J. Mankey, and F. J. Himpsel, Appl. Phys. Lett. **73**, 3459 (1998).
[45] V. Vlaminck and M. Bailleul, Science **322**, 410 (2008).
[46] K. Xia, P. J. Kelly, G. E. W. Bauer, A. Brataas, and I. Turek, Phys. Rev. B **65**, 220401(R) (2002).
[47] T. Kimura, T. Sato, and Y. Otani, Phys. Rev. Lett. **100**, 066602 (2008).
[48] M. Johnson and R. H. Silsbee, Phys. Rev. Lett. **55**, 1790 (1985).
[49] J. Z. Sun, Phys. Rev. B **62**, 570 (2000).
[50] W. Thomson, Proc. R. Soc. **8**, 546 (1857).
[51] M. I. D'Yakanov and V. I. Perel, Phys. Lett. A **35**, 459 (1971).
[52] N. Nagaosa, J. Sinova, S. Onoda, A. H. MacDonald, and N. P. Ong, Rev. Mod. Phys. **82**, 1539 (2010).
[53] Y. K. Kato, R. S. Myers, A. C. Gossard, and D. D. Awschalom, Science **82**, 1910 (2010).
[54] The difference between the used parameters and the original reported parameters in the experiment of Kimura *et al*. explains a factor 2 difference in the found spin-Hall angle.
[55] D. M. Rowe, *Thermoelectrics Handbook: Macro to Nano* (Taylor & Francis, London, 2006).
[56] R. D. Barnard, *Thermoelectricity in Metals and Alloys* (Taylor & Francis, London, 1972).
[57] L. Gravier, S. Serrano-Guisan, F. Reuse, and J.-Ph. Ansermet, Phys. Rev. B **73**, 024419 (2006).
[58] F. J. Jedema, Ph.D. thesis, University of Groningen, 2002.
[59] M. Cutler and N. F. Mott, Phys. Rev. **181**, 1336 (1969).
[60] G. Schmidt, D. Ferrand, L. W. Molenkamp, A. T. Filip, and B. J. van Wees, Phys. Rev. B **62**, R4790 (2000).
[61] H. Yu, S. Granville, D. P. Yu, and J.-Ph. Ansermet, Phys. Rev. Lett. **104**, 146601 (2010).
[62] M. Johnson and R. H. Silsbee, Phys. Rev. B **76**, 153107 (2007).
[63] J. J. A. Baselmans, A. F. Morpurgo, B. J. van Wees, and T. M. Klapwijk, Nature (London) **397**, 43 (1999).
[64] C. Kittel, *Introduction to Solid State Physics* (Wiley, New York, 1995).
[65] N. W. Ashcroft and N. D. Mermin, *Solid State Physics* (Brooks Cole, 1976).
[66] P. C. van Son, H. van Kempen, and P. Wyder, Phys. Rev. Lett. **58**, 2271 (1987).
[67] In practice, it is necessary to separate the creation and detection of a spin temperature in a lateral device in order to prove the effect is due to the spin temperature only. Otherwise, such effects can be mistaken for a spin-current injection related voltage spread over the detector interface. This geometry requires additional contacts which increases the distance between injection and detection and reduces the desired observable effect.
[68] S. S. P. Parkin, C. Kaiser, A. Panchula, P. M. Rice, B. Hughes, M. Samant, and S-H. Yang, Nat. Mater. **3**, 862 (2004).
[69] M. Tsoi, A. Jansen, J. Bass, W.-C. Chiang, V. Tsoi, and P. Wyder, Nature (London) **406**, 46 (2000).
[70] I. Krivorotov, N. Emley, J. Sankey, D. Kiselev, D. Ralph, and R. Buhrman, Science **307**, 228 (2005).
[71] S. Kaka, M. Pufall, W. Rippard, T. Silva, S. Russek, and J. Katine, Nature (London) **437**, 389 (2005).
[72] D. Houssameddine *et al*. Nat. Mater. **6**, 447 (2007).
[73] F. Albert, J. Katine, and R. Buhrman, Appl. Phys. Lett. **77**, 3809 (2000).